The CTOA as a Parameter of Resistance to Crack Extension in Pipes Under Internal Pressure

M Benamara, G Pluvinage, Julien Capelle, Z Azari

THE CTOA AS A PARAMETER OF RESISTANCE TO CRACK EXTENSION IN PIPES UNDER INTERNAL PRESSURE

M.Benamara[1], G.Pluvinage[2], J.Capelle[1], Z.Azari[1]

[1]LaBPS – ENIM, 1 route d'Ars Laquenexy, CS 65820, 57078 Metz, France
[2]FM.C 57530 Silly Sur-Nied, France

ABSTRACT

Different methods of CTOA measurements are described: Optical microscopy coupled with digital image correlation, analytical analysis of experimental load-displacement curves or simulation by Finite Element method. Using a Modified Compact Tension (MCT) specimen at room temperature, tests are performed to measure the value of the CTOA of API 5L X65 pipe steel. The influence of thickness on CTOA has been studied and explained through a "triaxial stress constraint". Crack extension is modelled by the finite element method using the CTOA criterion coupled with the node release technique. Crack velocity, arrest pressure and crack extension at arrest have been determined. Values of the CTOA are not intrinsic to materials. Like other measures of fracture toughness, it is sensitive to geometry and loading mode. This sensitivity can be described by a constraint parameter. For the thickness effect, the constraint parameter T_z is very appropriate.

1. INTRODUCTION

In fracture mechanics, the resistance crack to crack extension is generally expressed by the experimental crack growth resistance curve (i.e. the R-Curve). The crack driving force is expressed in terms of the stress intensity factor (SIF), J integral (J) or crack-tip opening displacement (CTOD) interconnected parameters based on the crack extension da. The crack-tip opening angle (CTOA), defined as the angle between two element sides representing the crack tip, is one of the latest ways to describe fracture resistance to crack extension.

Conditions of stable crack growth require that the rate of change of the crack driving force with increasing crack length Δa be smaller than the increase of crack growth resistance expressed in terms of crack opening displacement δ :

$$\frac{d\delta}{da} \leq \frac{d\delta_R}{da} \tag{1}$$

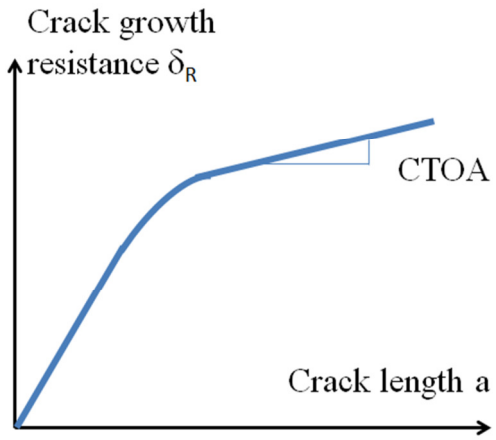

Fig. 1: Definition of CTOA on R curve $\delta_R = f(a)$.

It can be seen on the R curve $\delta_R = f(a)$ that the left term in (1) is precisely the CTOA that is constant in the linear part of the R curve (Fig. 1).

$$\frac{d\delta_R}{da} = CTOA \tag{2}$$

The concept of Crack Tip Opening Angle (CTOA) was probably introduced by Anderson in 1972 [1] to simulate stable crack growth by the Finite Element method (FEM). In this method, crack growth is obtained by successive relaxation of the nodal forces at the node representing the crack tip. The ψ angle as CTOA between two element sides representing the crack tip is chosen as the criterion for the crack extension. However, crack-growth dependence of this angle was expected, and a constant value was used for all of the stages of growth. The value at the first increment of crack growth is called ψ_0. Anderson assumed that after large crack growth, steady state conditions prevail and ψ stabilises to the ψ_c value with $\psi_c < \psi_0$. ψ_c is called the critical crack tip opening angle ($CTOA_c$).

Several authors [2-6] using two dimensional analyses, showed that CTOA at initiation is always larger than the value at stable crack growth (Fig. 2).

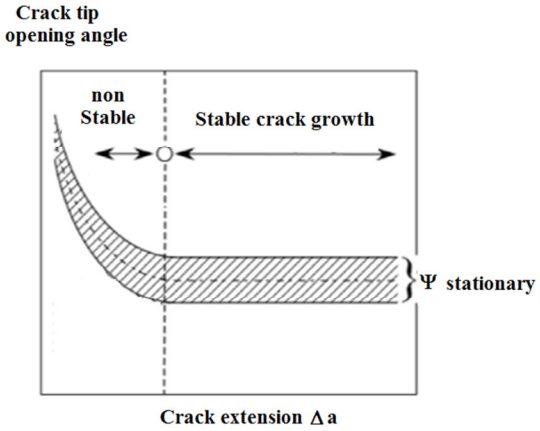

Fig. 2: Evolution of CTOA during crack extension.

Since the 1990s, the use of this criterion has been extended to numerical simulations by FEM of the crack extension.

Nowadays, $CTOA_c$ is used to predict crack length and pressure at arrest of a ductile running crack and particularly in gas pipes [7].

Gas pipeline fracture initiation is usually followed by extended running crack propagation. This occurs when driving force energy, caused by internal pipe pressure, overcomes the crack propagation resistance. Such disasters lead to significant financial loss, and should be avoided as much as possible or confined to a short portion of the pipe. Therefore, an important question is whether and when the fracture will self-arrest.

Conditions for crack propagation or arrest are given by a coupled fluid-structure problem. Depressurisation due to crack opening will cause fluid egress from the pipe. This induces a depressurisation wave propagating in the opposite direction to the tips of the opening crack. Crack propagation speed is controlled by pressure distribution of the opening pipe. If the decompression wave is faster than the propagating crack fracture, the pressure at the crack tip will decrease, and the crack arrests.

In terms of a limit state design, the arrest pressure can be predicted by solving Equation (3) between the fracture resistance and component stress, which depend on the pipeline dimensions, internal pressure and material strength. This material resistance is balanced with a component stressing that is determined involving specific pipe dimensions, pressure p and material strength. In terms of a limit state design, the arrest pressure can be predicted by solving the equation between the stress state at crack tip:

$$\langle \sigma_{ij}(p) \rangle = \langle \sigma_{ij,c}(p_{ar}) \rangle \tag{3}$$

where p_{ar} is the pressure at arrest. Condition of arrest can be transformed by the new following condition:

$$CTOA\ (p) = CTOA_c\ (p_{ar}) \tag{4}$$

where CTOA is the crack tip opening angle induced by the current pressure and $CTOA_c$ the fracture resistance.
In the standard codes for gas transmission pipelines, the toughness requirement for crack arrest is based on models that express the fracture resistance and driving force in terms of the fracture and gas decompression wave velocities. This approach involves the superposition of two curves: the gas decompression wave speed and the ductile fracture propagation speed characteristic, each as a function of the local gas pressure. For this reason, it is called Two Curves Method (TCM).
In the present work, the crack arrest criterion, given by Equation (4), is extended to the two-curves method through an FEM simulation model in conjunction with the node release technique. This method is used for the prediction of crack velocity, pressure at arrest and crack length after arrest by numerical simulation on pipe steel API 5L X65. A comparison has been made with the TCM codes for crack arrest [8].

2. EXPERIMENTAL DETERMINATION OF CTOA ON API 5L X65 PIPE STEEL

2.1 Definition

The CTOA is defined as the angle between the crack faces of a growing crack. A practical realisation of this definition is not possible because the crack faces are not straight but curved with a curvature that depends on the specimen and loading type. A definition based on crack tip opening displacement δ at a distance d of the order of 1 mm is consistent for both experimental and numerical determination (Fig. 3).

$$\Psi = arctg\left(\frac{\delta}{2d}\right) \tag{4}$$

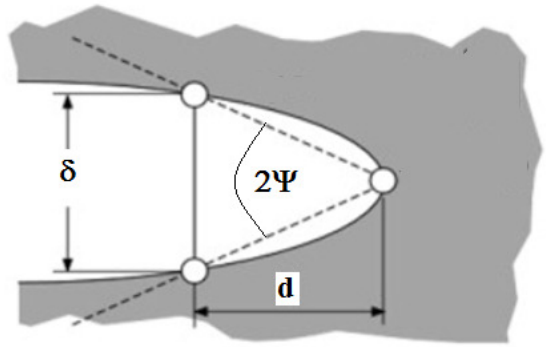

Fig. 3: Definition of CTOA on the curved crack profile.

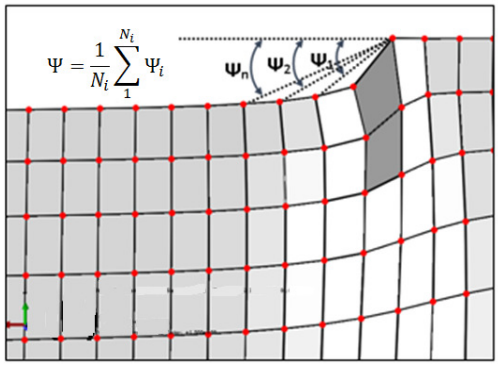

Fig. 4: Definition of CTOA according to the meshing crack.

In order to overcome the zigzag pattern of real crack faces or the influence of mesh size, it is more convenient to determine CTOAs at several distinct complementary positions on the upper and lower crack surfaces, ψ_i, and to average over these values afterwards (Fig. 4). The points used to determine the ψ_i values should be chosen in the range of 0.5–1.5 mm behind the crack tip.

$$\Psi = \frac{1}{N_i}\sum_{1}^{N_i}\Psi_i \tag{5}$$

2.2 Choice of specimen to determine CTOA

Different specimen types can be used for experimental determination of CTOA. Specimens loaded by bending are generally chosen because the specimens are smaller and need less material and less testing

capacity. The choice of aspecimen loaded by bending leads to the risk of crack bifurcation, which is not compatible with a CTOA measurement over a large crack extension.
Cotterel [9] pointed out the role of T stress in crack bifurcation. The T stress is a stress that acts parallel to the crack direction. Therefore, this stress combined with the opening stress induces a mixed mode of loading with a biaxiality ratio Θ :

$$\Theta = \frac{T\sqrt{\pi.a}}{K_I} \tag{6}$$

The maximum stress along the $\sigma_{\theta\theta}$ distribution is not always null for $\theta = 0$ and angular deviation can occur only for positive values of T stress. When the T stress is negative, the maximum $\sigma_{\theta\theta}$ is always along the direction of propagation $\theta = 0$.

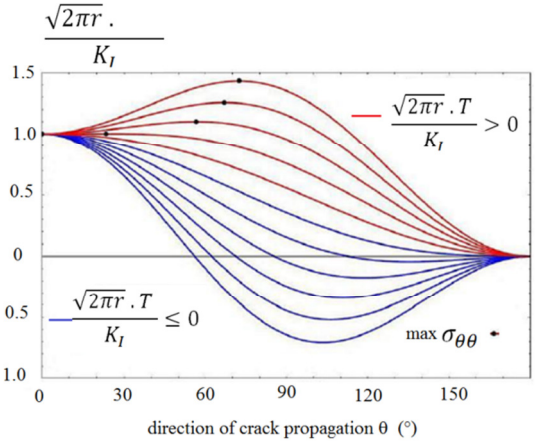

Fig. 5.Evolution of the ratio $\frac{\sqrt{2\pi r}\,.\sigma_{\theta\theta}}{K_I}$ with crack propagation direction θ in the presence of T stress.

If T stress is positive, the crack curves according to the criterion of maximum tangential stress introduced by Erdogan and Sih [10]. By applying this criterion, the opening stress is given by:

$$\sigma_{\theta\theta} = \frac{K_I}{\sqrt{2\pi r}}\left[\frac{3}{4}\cos\frac{\theta}{2} + \frac{1}{4}\cos\frac{3\theta}{2}\right] + T\sin^2(\theta) \tag{7}$$

$$\frac{\sqrt{2\pi r}\,.\sigma_{\theta\theta}}{K_I} = \left[\frac{3}{4}\cos\frac{\theta}{2} + \frac{1}{4}\cos\frac{3\theta}{2}\right] + \frac{T\sqrt{2\pi r}}{K_I}\sin^2(\theta) \tag{8}$$

The evolution of the ratio $\frac{\sqrt{2\pi r}\,.\sigma_{\theta\theta}}{K_I}$ with the direction of propagation θ is plotted in Fig. 5 for positive or negative values of T. The maximum opening stress is indicated by a black spot only for positive T stress. For negative T stress, this maximum occurs for negative values of opening stress and bifurcation cannot occur because the crack surfaces cannot overlap [11]. The bifurcation angle $\theta^*$is given when the first derivative of Equation (9) is equal to zero and the second derivative must be negative.

$$\theta^* = \cos^{-1}\left[\frac{1 + \sqrt{1 + \frac{1024\pi}{9}.X_{ef}.\left(\frac{T_c}{K_{Ic}}\right)^2}}{\frac{512\,\pi}{9}.X_{ef}.\left(\frac{T_c}{K_{Ic}}\right)^2}\right] \tag{9}$$

Introducing a local fracture criterion in this analysis for which at fracture $K_I = K_c$, $T = T_c$ and $\sigma_{\theta\theta} = \sigma_c$ for $x = X_{ef}$ allows us to compute the bifurcation angle θ^*. X_{ef} is the size of the fracture process volume or effective distance. The condition on the second derivative implies that for crack curving :

$$\frac{T_c}{K_c} > \frac{3}{8}\frac{1}{\sqrt{2\pi X_{ef}}} \tag{10}$$

We now compare the potentiality of crack curving of two specimens: the first is a classical compact tension (CT) specimen with 10 mm thickness; the second a modified CT specimen (MCT) with the same thickness.

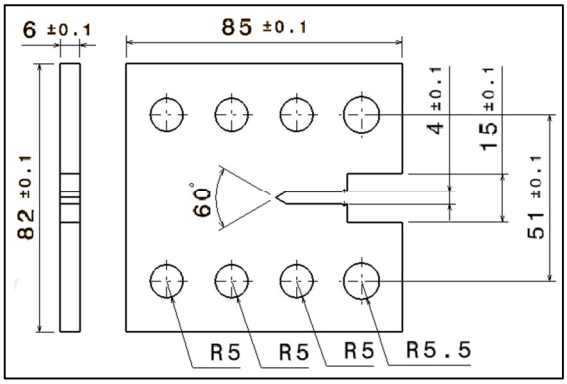

Fig. 1 : Geometry and design dimensions of modified CT (MCT) specimen.

The geometry of the MCT specimen is given in Fig. 6 and is similar to the geometry of the specimen used by Darcis et al [12]. T stress has been computed by FEM versus non dimensional crack size a/W assuming a linear behaviour. Results are reported in Fig. 7.
For negative T stress, after initiation, the crack propagates first in an unstable manner and secondly, after several millimetres, in a stable manner.

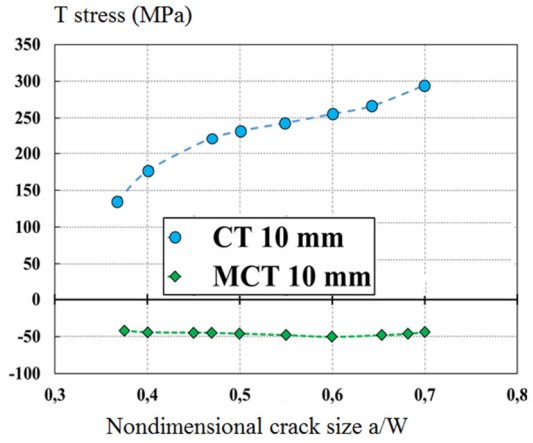

Fig.7 : Evolution of T stress with non-dimensional crack size for a CT and an MCT specimen.

Fig. 8: Crack bifurcation in CT specimen with positive with positive T-stress-induced crack curving T/K= + 2.05 X_{ef} = 0.49 mm

During crack propagation in a stable manner, the crack tip opening angle CTOA remains constant and its constant value is considered a characteristic of the fracture resistance of the material to crack extension. It can be noted that during the stable crack propagation both CTOA and T stress are constant [13]. T stress is negative for the MCT specimen and practically constant with an average value T_{CT} = -45 MPa. For the CT specimen, T stress increases with a/W ratio and its value for a/W = 0.5 is T_{MCT} = 220 MPa. The positive value of T stress explains the crack bifurcation that can be seen on Fig. 8. Therefore the MCT specimen with a negative T stress is more appropriate to determine CTOA.

2.3 Different methods of measurements of CTOA

Various methods are used for experimental determination of the CTOA. They can be divided into two categories: direct and indirect methods. Direct methods comprise *micro-topography* [14], optical microscopy coupled with image correlation method [15–16]. Indirect methods are based on the analysis of the load displacement diagram, either numerically [17] or analytically [18–19].

2.3.1 Direct methods

In *micro-topography* [14], the fracture surfaces are topographically analysed *post-mortem.* This method is based on the assumption that the CTOA is preserved in the plastic deformations of the fracture surface. After both surfaces have been scanned, they are recombined in the computer. The reconstructed crack contours at fracture allow the determination of the CTOA. This method is of interest because it allows the CTOA to be identified in positions of different thicknesses, but it is time consuming.

Optical microscopy is one of the most common methods of measuring *CTOA* [20]. The crack contour close to the crack tip is investigated at the polished surface using a light microscope. A special case of optical measurement is the digital image correlation (DIC) method. For our measurements, a commercial DIC camera (Gom FASTCAM SA.1 Photron) and a software analysis package with integrated length and angle measurement tools (ARAMIS V6.3) have been used to measure CTOA and crack extension Δa. The recording time was automatically available from the videotapes, where a digital stopwatch was used to synchronise the still images. All of this allowed test parameters such as load, displacement, and crack length Δa to be correlated with CTOA. One example of such a digital image and the corresponding CTOA values is given in Fig. 9.

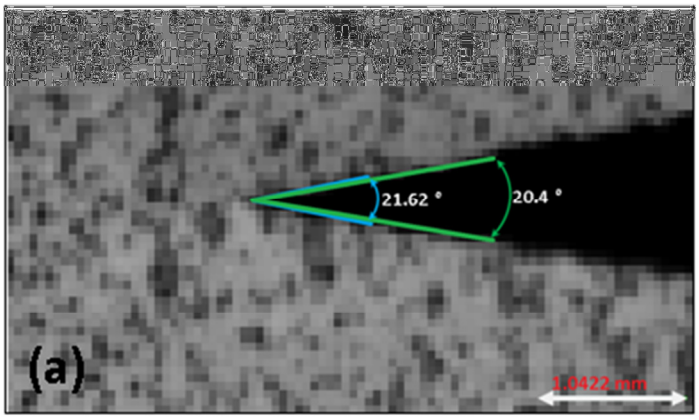

Fig. 9: Digital image of a crack and corresponding CTOA values.

Two methods are used to determine the CTOA value :

The first method (Method 1) requires the use of an algorithm to locate the crack front, on the studied image and for selecting the pairs of points along the crack profile with imposed distances (Fig 10a). The pairs of points allow us to obtain series values $CTOA_i$ using the following formula:

$$CTOA_i = \left.\frac{\delta_i}{L_i}\right|_{\Delta a} \quad [rad] \tag{11}$$

where δ_i is the distance between two points of coordinates i and L_i the distance between the crack tip and point with coordinate i. $CTOA_i$ are averaged to obtain $\overline{CTOA}_{\Delta a}$ value for a given crack extension Δa .

The second method (Method 2) requires also the use of an algorithm and the selection of pairs of points along the crack profile as the first method, (Fig. 10b). In this method, the position of crack tip that is often difficult to localise is not necessary, and the point of coordinates i=0 is used. Series values $CTOA_i$ are obtained using the following formula:

$$CTOA_i = \left.\frac{\delta_i - \delta_0}{r_i}\right|_{\Delta a} \quad [rad] \tag{12}$$

r_i is the distance between the crack tip and points with coordinates i and δ_0 is the distance between two points of coordinates i = 0. As previously, the average value gives the $\overline{CTOA}_{\Delta a}$.

This method is preferred since it does not need crack tip localisation and leads to less scatter. The two methods have been compared with a series of 4 tests named (a, b,c and d) on CT specimen made from pipe steel X65. The two methods give similar values of CTOA. However the standard deviation is higher for method 2. Therefore, method 1 has been used in the next for CTOA measures on MCT specimens.

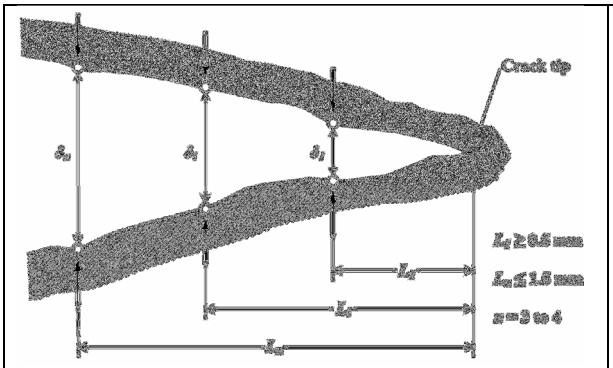

Fig 10: methods for determining $\overline{\mathrm{CTOA}}_{\Delta a}$ using crack tip location

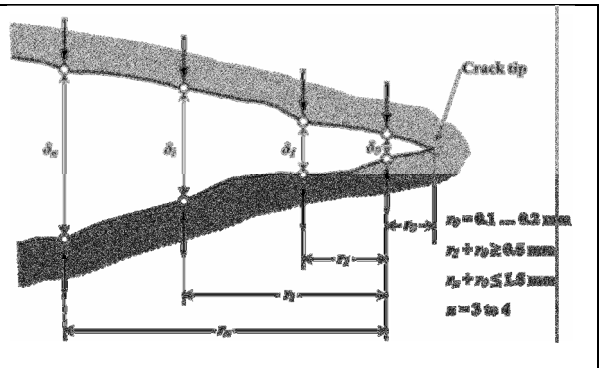

Fig 11: methods for determining $\overline{\mathrm{CTOA}}_{\Delta a}$ without using crack tip location

Table 1: mean and standard deviation for CTOA measurement on CT specimens made in pipe steel X65. Comparison of methods 1 and 2.

	Method 1		Method 2	
Specimen test	a	b	c	d
mean	18.3°	17.5°	20.5°	18.1°
Standard deviation	2.9°	1.3°	4.7°	3.2°

2.3.2 Indirect methods

These methods are based on the simulation by Finite Element Analysis or analytically of the load displacement diagram. Analytical analysis of experimental load-displacement curves in order to determine the CTOA can be carried out using different assumptions. The first one considers that the material has the stress-strain behaviour of an elastic perfectly plastic material. The second assumption considers that the material is strain hardening and the stress strain curve is described by a key curve. The third introduces the real stress strain curve in a finite element code.

Xu et al. [21] developed a method derived from the plastic hinge ductile fracture model [23] called the "simplified single-specimen method" (SSM). This model employs a regression algorithm of logarithmic load against displacement, avoiding the determination of crack extension and removing the requirements of material-based parameters. It is assumed that the ligament is fully yielded and the specimen rotates around a fixed centre of rotation at a distance of r*(W – a) = r*b from the crack tip (Fig. 12), where r* is the rotation constant, b the ligament size, a the crack length and W the specimen width. Neglecting the small change in position of the centre of rotation for a small increment of crack length, the half crack-tip opening displacement can be related to a small increment of rotation angle (dα) by:

$$\frac{\delta}{2} = r * (W - a) d\alpha \tag{13}$$

From these relations, CTOA can be written as

$$tang\, \Psi/2 = \mathrm{r} * \mathrm{b} \frac{d\alpha}{dy} \tag{14}$$

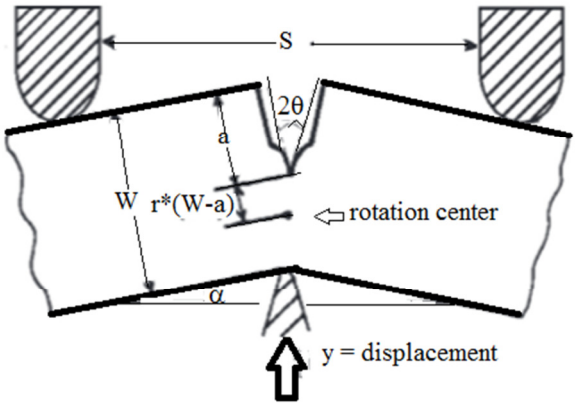

Fig. 12: Mechanisms of plastic deformation of a 3PB specimen assuming the existence of a rotation centre.

Assuming that the material has a perfectly plastic behaviour, the limit moment M_L of a 3PB specimen is given by:

$$M_L = \frac{P_L S}{4} \tag{15}$$

where P_L is the limit load and S the span. The limit load is given by:

$$P_L = \frac{4AR_c Bb^2}{S} \tag{16}$$

where A is a geometrical constant that depends on the stress state, R_c the flow stress, b the ligament size and B the thickness. During the crack extension increment Δa, the limit load decreases by ΔP_L, the specimen arms rotate by dα and the deflection y increases by dy. The derivative of the limit load is given by:

$$dP_L = \frac{8AR_c Bb}{S}\, db = \frac{8AR_c Bb}{S}.\left(-\frac{r*b}{tang\,\Psi/2}d\alpha\right) = \frac{8AR_c Bb}{S}.\left(-\frac{r*b}{tang\,\Psi/2}\frac{2dy}{S}\right) \tag{17}$$

with db = -da and $d\alpha = \frac{2dy}{S}$. By substituting dα into (12), one obtains:

$$dP_L = -\frac{4r*P_L}{Stang\,\Psi/2}\, dy \tag{18}$$

By rearrangement:

$$\frac{dLnP_L}{dy} = -\frac{4r*}{Stang\,\Psi/2} \tag{19}$$

The LnP_L versus $(y - y_{max}/S)$ curve may be used to evaluate Ψ, requiring values only for r*. Constancy of the slope implies constancy of the CTOA.

$$\psi\,(°) = 2.180/\pi\; arctang((-4r*)/((dLn(P))/dy)) \tag{20}$$

An example of such an evaluation of CTOA from a Charpy test of X65 pipe steel is given in Fig. 13.

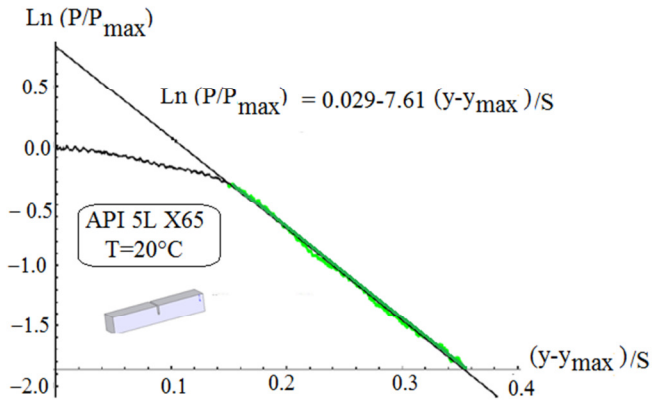

Fig. 13: Example of simplified single-specimen method (SSM) applied to a Charpy specimen made of X65 pipe steel.

Moreover, this method is strongly dependent on the reliability of the limit bending load hypothesis. In addition, strain hardening is not taken into account. For this reason, Fiang et al. [24] evaluated the crack extension according to the procedure of the key-curve method, where load and displacement are related according to:

$$\frac{PW}{b_0^2} = m\left(\frac{y}{W}\right)^n \tag{21}$$

where W is the width, b_0 the initial ligament size, and m and n are constants. The key curve is analytically established by fitting the original relationship between the load P and the displacement y on the pre-peak part of the instrumented test curve. After obtaining the parameters m and n, the amount of crack extension is estimated at any displacement on the post-peak part of the force-displacement curve, as:

$$\Delta a = W - \left[\sqrt{\left(\frac{PW^{n+1}}{my^n}\right) + a_0}\right] \tag{22}$$

Combining (21) and (22),

$$\frac{tang\Psi}{2} = \frac{-2r*}{S}\frac{dy}{dLn(W-a)} \tag{23}$$

The $\Delta Ln(W-a)$ versus ($y - y_{max}/S$) curve may be used to evaluate Ψ, requiring values only for r*.

$$\frac{tang\Psi}{2} = -2r* \frac{d[(y-y_{max})/s]}{\Delta Ln(W-a_0-\Delta a)} \tag{24}$$

These two methods have been compared with a series of 3 tests named A, AA and AAA on Charpy V specimens made in pipe steel X65. Results are presented in Table 2. The load-displacement is simulated with the Abaqus software through a subprogram called "routine". Once this curve is published in code, an algorithm will compare the numerical and experimental responses. The following condition is introduced: the numerically calculated load cannot exceed the experimental load level. A node release action is taken as soon as this condition is met. This node release simulates the crack extension and reduces the load level.

Table 2 : CTOA measurement on Charpy V specimens made in pipe steel X65 from load-displacement curve. Comparison of Equations (20) and (24).

Charpy test	A	AA	AAA
CTOA Equation (20)	22.0°	24.0 °	24.0°
CTOA Equation (25)	21.7°	23.8°	23.7°

In the second step, the R curve is obtained from crack driving force (SIF or COD) deduced from simulated load versus crack extension deduced from node release technique. This curve is fitted by a power relationship and CTOA deduced from Equation (2). This method is called the "Combining Numerical Method" (CNM).
With intent to validate this tool, we compared the numerical measures of CTOA to those provided by the direct method, Figure 14. Unlike DIC, it does not allow the identification of the zone of instability that preceded the stable crack extension with high values of CTOA. CNM detects the rapid decrease of CTOA reported in the literature. However the difference in the zone of unstable crack extension, the two methods are in good agreement in the range of the studied crack extension. The second method provides more advantages in accuracy, and in its easer implementation.

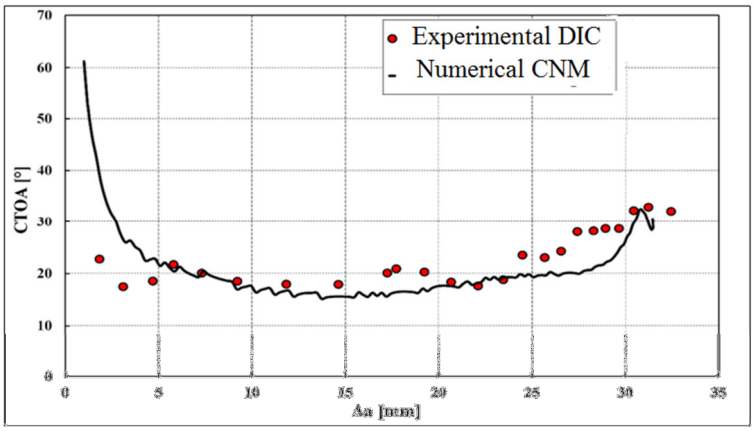

Fig. 14: Comparison of CTOA versus crack extension curve obtained by CNM and the DIC method for a modified CT specimen made of X 65 pipe steel

2.4 CTOA value at stable crack growth for an X65 pipe steel

The investigated material is an API 5L X65 grade pipeline steel supplied as a seamless tube with a wall thickness equal to 19 mm and external diameter of 355 mm. The mechanical properties, measured at room temperature on three tensile test specimens in the circumferential direction, are given in Table 3.

Table 3. Mechanical properties of pipeline steel API 5L X65 at 20 °C.

Yield stress σ_y [MPa]	Ultimate strength σ_{ul} [MPa]	Elongation at failure A [%]	Charpy energy K_{CV} [J]	Fracture toughness K_{Jc} [MP$\sqrt{}$am]
465.5	558.6	10.94	285.2	280

Using a Modified Compact Tension (MCT) specimen at room temperature, tests are performed to measure the value of the CTOA during crack extension. The geometry and dimensions of the test specimen are shown in Figure 6. The study specimens were pre-cracked to provide an initial ratio of crack length to specimen width of a/W = 0.4 using a fatigue stress ratio R = 0.1. The sinusoidal loading oscillates at a frequency of 15 Hz and the maximum load is kept below 7.2 kN. According to ASTM (E 2472) [24] requirements, the CTOA measurements were made at a distance behind the crack tip ranging between 0.5–1.5 mm. CTOA was determined using optical microscopy and also by finite element fitting of the experimental load. In addition,

CTOA was also determined on a Charpy specimen using the simplified single-specimen method. Values obtained with the different methods are given in Table 4.
For all experimental tests, the CTOA versus crack extension behaviour consisted of an initially high CTOA region that quickly transitioned into a clearly constant CTOA region. The stable value of CTOA is called $CTOA_C$. Values of $CTOA_C$ of API 5L X65 pipe steel obtained with three different methods are reported in Table 4.

Table 4 : Values of $CTOA_C$ of API 5L X65 pipe steel obtained with three different methods.

Method	DIC (MCT)	CNM (MCT)	SSM (Charpy)
Ψc(°)	20.66	24.68	21.8

A lower bound of $CTOA_C$ is set as 20°. This value is compared to other values of $CTOA_C$ found in the literature (see Table 4).
We note that the values obtained are higher than other values found in the literature (Table 5).

Table 5: Values of $CTOA_C$ found in the literature and in the present study for API 5l X65 steel.

References	Yield stress [MPa]	$CTOA_c$[°]	Specimen
[25]	447	8.1	DWTT
[25]	529	14.2	DWTT
[26]	543	11.61	MDCB
[27]	460	11.0	MDCB
[27]	522	8.6	MDCB
Current study	465	20	M(CT)

2.5 Influence of Thickness on CTOA

It is now well known that fracture resistance decreases when the thickness increases However CTOA seems less affected by thickness 'Fig.15).. The fracture resistance is maximum for plane stress conditions and trends asymptotically to a minimum called K_{Ic} or J_{Ic} if the plane strain conditions are satisfied. The effect of thickness B on fracture toughness is introduced through a "triaxial stress constraint" T_z. This parameter is defined as:

$$T_Z = \frac{\sigma_{zz}}{\sigma_{yy} + \sigma_{xx}} \tag{25}$$

Table 6: Triaxial stress constraint T_z values with pipe thickness for a pipe diameter of 355 mm.

Wall thickness [mm]	T_z
Plane stress	0
6 (this study)	0.204
10	0.2629
15	0.3109
19	0.335
Plane strain	9.52

For a straight through-thickness crack, which is a typical case of 3D cracks, y is the direction normal to the crack plane xoz. In an isotropic linear elastic cracked body, T_z ranges from 0 to N, $T_z = 0$ for the plane stress state, and $T_z = N$ for the plane strain state. N is the strain hardening exponent of the Ramberg-Osgood strain-stress relationship. Values of T_z for different pipe thicknesses and for the same pipe diameter of 355 mm are reported in Table 6 and compared to plane stress or plane strain stress states. We note the low value of T_z for the MCT specimen used in this study. A combined effect of constraint and thickness can explain the lower values of CTOA found in the literature.

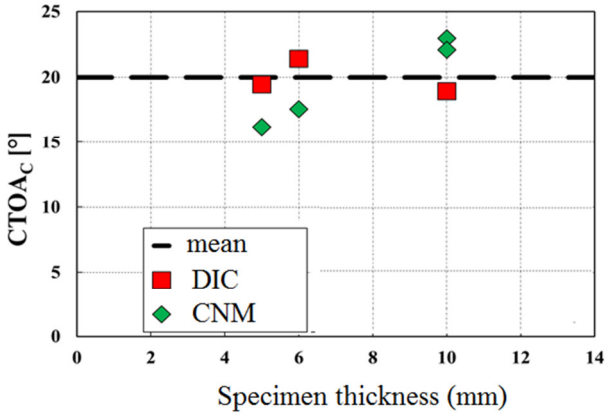

Fig. 15: Influence of thickness on critical CTOA. API5L X65 pipe steel.

3. NODE RELEASE TECHNIQUE FOR CRACK EXTENSION

The modelling of crack propagation using CTOA has been the subject of several studies [28–30]. Crack extension is modelled by the finite element method using the CTOA criterion coupled with the node release technique. The node release technique algorithm has been presented in an earlier study [11]. It is based on the assumption that cracks grow step by step, and each step has the length of one mesh element.

This approach needs implementation in FE code without any particular problems. In this work, this has been made on Abaqus 6.11 code with the node debonding option called "Debond". Implementation of the CTOA approach is made using the subroutine “User Subroutine” associated with the finite element solver Abaqus. This programming task is divided into two major steps:

The first step is to develop a routine that allows the identification of the crack tip and evaluating CTOA during the calculation. To accomplish this step, the Abaqus solver is associated with the subprogram "URDFIL".

The second step is to modify the crack surfaces during each resolution step. This can be done by releasing representative node of the crack tip. This node release task is performed via the subroutine "MPC" (Multipoint Constraint Subroutine).

In addition, it is necessary to identify the crack tip and all necessary nodes for evaluation CTOA of each computing increment. Evaluation of CTOA during the progression of calculations is made by a subroutine "URDFIL". To simplify this task of identification, the mesh used in the simulation is adapted. In order to do that, the representative nodes of the crack path are incremented starting from the crack tip with respect to the direction of crack extension.

The subprogram "URDFIL" imports data from a results file at the end of each computing increment calculation. This allows us to know the coordinates of each node and to evaluate CTOA through a vectorial computing program, according to Equation (26).

$$\mathrm{CTOA}=\sum_{j=1}^{m}\left(\sum_{i=2}^{n} ACos\left[\frac{\left(X_1^j-X_i^j\right)^2+\left(Y_1^j-Y_i^j\right)*\left(Y_1^j+Y_i^j\right)+\left(Z_1^j-Z_i^j\right)^2}{\sqrt{\left(X_1^j-X_i^j\right)^2+\left(Y_1^j-Y_i^j\right)^2+\left(Z_1^j-Z_i^j\right)^2}}\right]/n\right)/m \qquad (26)$$

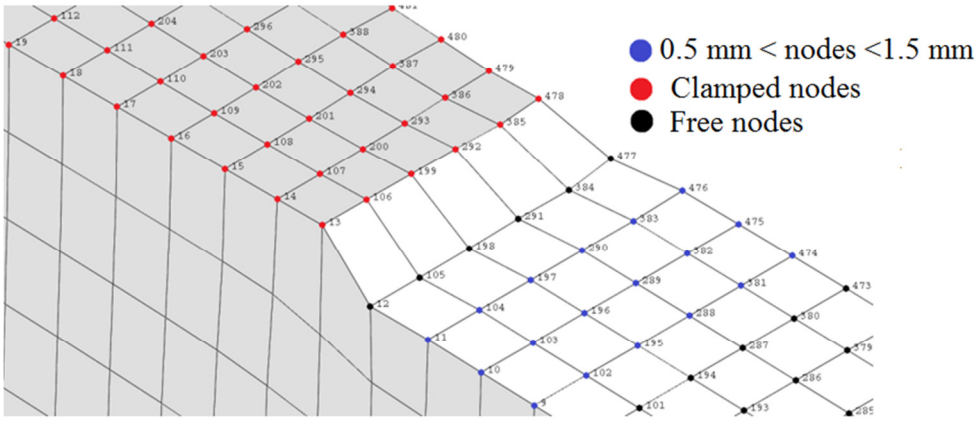

Fig 16 : The node release technique configuration of debonded and fixed nodes.

The MPC (Multi-Point Constraints) method with ABAQUS (version 11.6), made possible the implementation of the node release technique in a three-dimensional simulation. The MPC method involves a special mesh. Unlike a conventional mesh that uses a node at each corner of element, four nodes are located at identical coordinates. The nodes a, b, c and d of the four elements A, B, C, and D are coupled together. This means that their movements are forced to be the same. To create a new crack surface, it is necessary that these nodes be able to separate Fig.16. This separation process needs the debonding of one or two nodes at the same time. According to the chosen node, crack extension has three possible directions. This operation can be represented by the following equation

$$\begin{pmatrix} k_1^1 & k_2^1 & k_3^1 & k_4^1 \\ 0 & k_1^2 & k_2^2 & k_3^2 \\ 0 & 0 & k_1^3 & k_2^3 \end{pmatrix} \begin{pmatrix} u_a \\ u_b \\ u_c \\ u_d \end{pmatrix} = \begin{pmatrix} 0 \\ 0 \\ 0 \end{pmatrix} \qquad (27)$$

whereu_a,u_b,u_c etu_d are displacements of nodes a, b, c et d. $k_i^j$are scalars with values 0, 1 or -1, according to crack extension direction.

Two increment strategies are available in the ABAQUS code: automatic and fixed. Computing has been made according to both strategies. The ratio accuracy/computing time has been used as the criterion of choice of the most appropriate strategy. Results are reported in Table 7. It is obvious that the strategy of a fixed increment reduces the computing CTOA, but this involves a considerable calculation time. To overcome this difficulty, a hybrid strategy has been used. The solver ABAQUS automatically manages the computing step size until a CTOA amplitude reaches a value equal to than 80% of CTOAc. Then the subprogram "URDFIL" takes over to reduce the increment size gradually to the critical value of CTOA.

Table 7 : Computing time and error according to increment strategies automatic or fixed

Incrementation strategy	Error [°]	Error [%]	Number of increments	Computing time [h]
automatic	0,365	1,85	2178	2h27
Fixed	0,076	0,38	6325	7h33

Mesh dependence was checked with three different 3D meshes. The results presented in Table 8 indicate that a good convergence can be obtained by observing a minimum level of mesh refinement. This level may be related to the definition of the CTOA and the maximum size of an element cannot exceed 1.5 mm.

Table 8: Influence of mesh type on error and computing time.

Mesh	Mesh type	Nodes number	Error [%]	Computing time [h]
1	C3D8R	22008	5,95	2h26
2	C3D8R	33612	5,8	4h17
3	C3D8R	55513	3,74	7h23

4. FINITE ELEMENT MODELLING OF CRACK EXTENSION

4.1 Meshing

The modelling task begins with the three-dimensional mesh of the geometry of the pipeline. Owing to symmetry, only ¼ geometry is analysed to reduce the computation time further. Two zones of meshes were generated: a first fine mesh zone along the crack plane with an element size equal to 1.4 mm, and a second coarse mesh with an average size of 15 mm; see Fig. 17.

The connection between the two mesh regions is performed under ABAQUS which allows the connection of the solid type of surface. The final step of meshing is to name the crack plane nodes by the procedure described previously allowing the identification of the crack tip and calculation CTOA in its vicinity. A total of 50976 eight node, hexahedral elements were generated along the crack path and combined with 6000 shell elements.

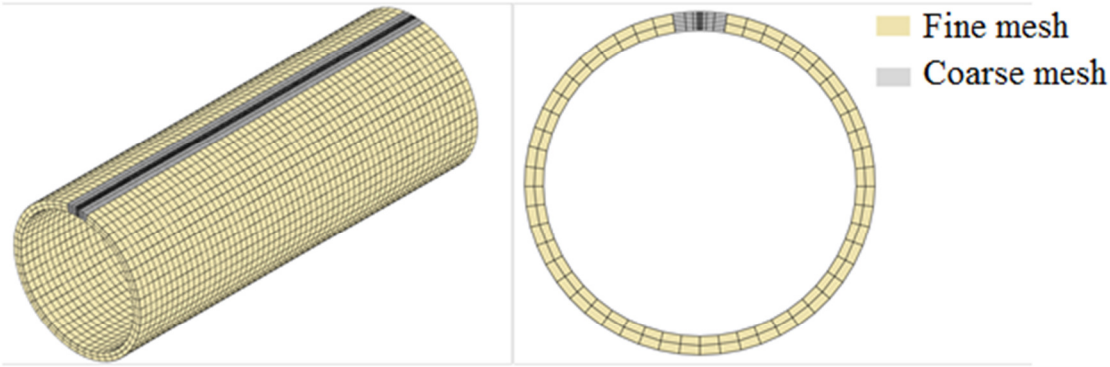

Fig 17 : Mixed mesh for a pipe and a running crack.

4.2 Boundaries conditions:

Conditions of crack symmetry in the $\vec{x}$ direction allow the removal of two rotations along the $\vec{y}, \vec{z}$ axes and the displacement in the $\vec{x}$ direction. By analysing only ¼ of the pipeline, a symmetry condition in the $\vec{y}$ direction is imposed to the central plane of the pipeline. The end of the pipeline is assumed to be clamped.

4.3 Loading

Computing is made by applying a gradual pressure on the inner surface of the pipeline. During the computing progress, the CTOA value increases until it reaches its critical value $CTOA_c$. Then, the node releasing subroutine applies the release action of crack tip nodes, which leads to crack extension.

To fulfil the conditions of energy balance, the node release action is associated with a decrease of the loading level. A third sub-program type "DLOAD" reduces by 2% the pressure on the inner wall of the pipeline following each node release action. Under this same routine and as close as possible to the actual conditions of a burst test. According to the assumption of Maxey et al. [31], only the portion of the pipeline downstream of the crack tip is constantly charged by the gas pressure. Using this same routine, the internal pressure is imposed to a certain distance ahead of the crack tip. This distance is estimated from a model based on the cohesive zone model of Dugdale-Barenblatt [32]. In this model, the distance over which the internal pressure is applied is based on the dimensions of the pipeline:

$$2b = 3\sqrt{R.t} \tag{28}$$

where R and t are the outer radius and thickness of the pipeline, respectively.

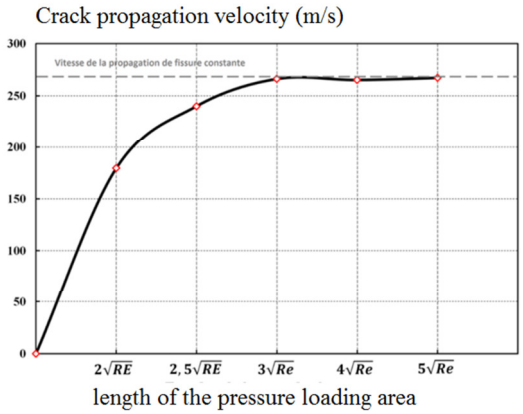

Fig. 18: Influence of distance ahead of the crack tip where internal pressure is imposed

In order to check Maxey's assumption, we have studied the influence of the extent of the applied pressure zone on the rate of crack propagation. Five simulations at an internal pressure of 40 MPa and for different lengths $2b = h\sqrt{Rt}$ where h is a factor that takes values [2, 2.5, 3, 4 and 5], have been performed. The crack propagation velocity versus $h\sqrt{Re}$ is reported in Table 9 and Fig. 18. We justify the choice of the length 2b according to Equation (28).

Table 9 : influence of h parameter on crack extension velocity.

h	2	2.5	3	4	5
V_c(m/s)	180	240	266	263	262

4.4 Strain rate effect

The crack propagation following the burst of the pipeline is a dynamic phenomenon. A strain rate that amounts to more than 1500 s^{-1} was measured in the vicinity of the crack tip according to the results reported by Oikonomidis et al. [33]. Thus, the influence of the strain rate is necessary taking into account in the numerical model through the dynamic behaviour law of Johnson Cook:

$$\sigma_{eq} = (A + B{\varepsilon_{eq}}^{n})(1 + Cln\left(\frac{\dot{\varepsilon}_{eq}}{\dot{\varepsilon}_0}\right) \quad (29)$$

whereσ_{eq} is the equivalent von Mises stress, ε_{eq} the equivalent strain, $\dot{\varepsilon}_{eq}$ equivalent deformation rate and $\dot{\varepsilon}_0$ the reference strain rate . A, B, C and n are the Johnson Cook parameters. These parameters for API 5L X65 pipeline steel, have been reported by Jakobsen [34]: Table 10.

Numerical results obtained with and without the strain rate dependence indicates a small influence on crack speed in pipes made of API 5L X65 steel with a variation of the crack growth rate of less than 5%. This is explained by the low strain rate sensitivity of the API 5L X65 steel [34]. However despite the minor influence of the crack velocity, the influence of strain rate is taken into consideration in order to build a more accurate model.

Table 10 : Johnson Cook parameters for API 5l X65 pipe steel [34].

Material parameters	A (MPa)	B (MPa)	n	C	$\dot{\varepsilon}_0$ (s^{-1})
	465.5	410.83	0.4793	0.0104	0.000806

At the time of the occurrence of a through crack in the pipeline, the gas escapes through the created opening and provokes a sudden decompression that consists of two decompression waves running along the pipeline at a speed of the order 300 m/s. These opposed waves play an important role in the dynamics of failure.
Indeed, if the propagation rate of the decompression wave is lower than the crack speed, the crack tip will be continuously loaded at the initial pressure. An infinite stationary crack propagation occurs. On the contrary, the crack is gradually discharged until arrest.
In order to predict the velocity of the decompression wave of the gas, numerous models have been developed based on the Finite Difference Method, the Characteristics Method, or an experimental method such as the shock tube test. These methods generally assume a one-dimensional flow (along the axis of the pipe) and isentropic gas behaviour. According to Civallero et al. [35] and in the case of a pure gas phase, the pressure in the vicinity of the crack follows the following relationship:

$$V_c > V_d p_l = p_0$$

$$V_c < V_d p_l = p_0 \left[\left(\frac{2}{\gamma+1}\right) + \left(\frac{\gamma-1}{\gamma+1}\right).\frac{v_c}{v_d}\right]^{(2\gamma/\gamma-1)} \quad (30)$$

where V_c and V_d are, respectively, the crack and decompression wave speed, p_0 and p_l, initial and leak pressures, γ ratio of specific heats of the gas (iso-pressure and isochore).

Cheng et al. [36] studied the decompression of supercritical CO_2 through shock tube tests and numerical simulations with the calculation code GASDECOM [37]. A simplified gas depressurisation model similar to Cheng et al.'s solution is used in this work and assumes that the gas decompression pressure depends only on time and distance from the crack tip and that the crack propagation cannot outrun the decompression wave. The expansion of the ideal gas is isentropic, and the pipe is considered as a large pressure vessel with constant volume. The pressure drop ahead of the running crack tip is given by the following equation:

$$p(t) = p_0.\exp(kt) \quad (31)$$

where k is a constant k = -7.5 s^{-1} [37] that can be related to the gas parameters and initial conditions of pressure and temperature.

5. RESULTS

Crack extension modelled by the Finite Element method using CTOA criterion coupled with the node release technique allows us to predict the crack velocity, the arrest pressure and crack length. It has been applied for a pipe with wall thickness equal to t = 19 mm and external diameter OD = 355 mm made in API 5L X65 pipe steel.

5.1 Crack velocity

Crack extension from an initial crack like defect is computed using the described model. Running crack propagation along the tube consists of two stages: a boost phase where the crack reaches its full velocity in a few milliseconds, followed by a steady stage at constant speed. The absence of a deceleration phase is explained by the lack of gas decompression law in the model. One notes that the crack velocity increases with the initial pressure. Ten simulations were performed at different levels of pressure in the range 25–60 MPa. Results reported in Fig. 19 indicate that the stationary crack velocity V_c [m/s] increases with decompression pressure p_d in MPa according to :

$$V_c = 284.2 * (\frac{P_d}{25.8} - 1)^{0.193} \quad (32)$$

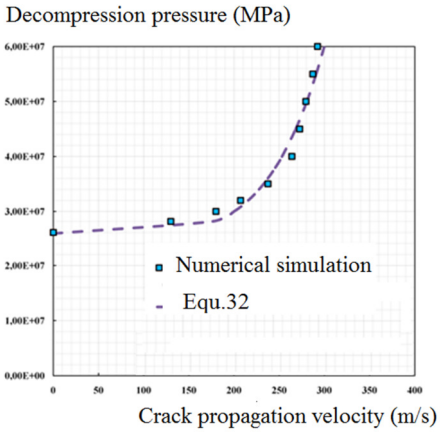

Fig. 19 : decompression wave versus crack velocity; pipe made of API5L X65, diameter 355 mm and thickness 19 mm.

5.2 Arrest pressure

The arrest pressure is defined relative to crack propagation and not arrest. Therefore it is considered as the minimum pressure level to ensure the steady crack propagation. Above this pressure p_{ar}, the crack propagates in an unstable manner and along a long distance. Under this value, the crack propagation will auto-arrest or propagate along a short distance. The arrest pressure is obtained using the CTOA Abaqus user subroutine within a static analysis.

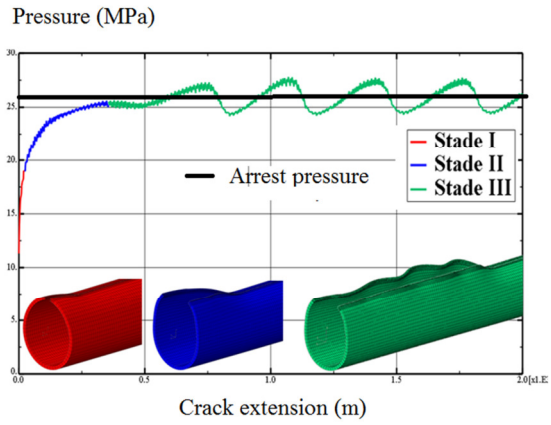

Fig. 20 : determination of arrest pressure by static analysis using CTOA Abaqus User Subroutine.

Evolution of the crack tip pressure travel is characterized by three stages (Fig. 20): first, the crack tip pressure experienced a sharp rise to a crack extension equivalent to the wall thickness of the pipeline, followed by a second and more gradual increase. Finally, the pressure converges to a relatively stable value during a third stage and is defined as the arrest pressure. The increase of the crack tip pressure is linked to increasing fracture toughness with crack extension, as described by the R curve concept. James et al. [38] assume that the increase of fracture toughness is related to the tunnel effect, and find that a crack propagates in an unstable manner along a distance equivalent to the thickness. Experimental tests on modified CT specimens in our experimental study of CTOA confirm this assumption.

During the second stage, the wall deformation of the pipe modifies the loading mode. Scheider et al. [39] indicate that during this transitional stage, crack propagation extension is about the same as the diameter of the pipeline.

The third stage is characterised by the stability of the crack tip pressure and no variation in the stress distribution near the crack tip. Although the crack propagation is stationary, we see waves in the pipe opening geometry at crack tip pressure near the arrest one. This is due to the local buckling phenomenon in bursting tests on pipelines made of X70 steeland analysed by Tran [40]. Tran links these ripples to the level of ductility of the material and nonlinear geometrical effects associated with modification of the load surface at the crack tip.

To define the arrest pressure, these waves are neglected and the mean value is considered. In the case presented in Fig. 17, the arrest pressure p_a = 25.8 MPa is obtained.

5.3 Crack extension at arrest

Crack extension at arrest is obtained from the graph crack velocity half of the crack extension to take into account the symmetry of the problem (Fig. 21). For the aforementioned conditions of geometry, material and initial pressure, the numerical simulation gives a crack extension of 42 m, which is of the same order of magnitude to those obtained experimentally.

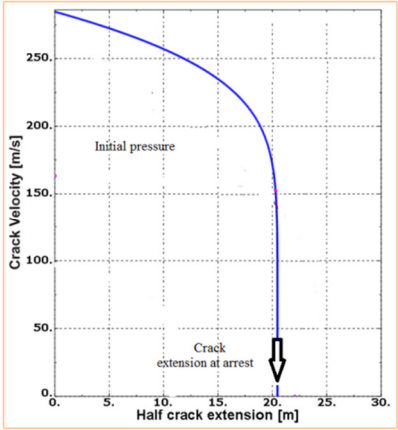

Fig. 21: Graph crack velocity half of the crack extension, determination of crack extension at arrest X65 pipe steel, initial pressure p_0 = 45 MPa.

6. DISCUSSION

The use of CTOA for prediction of dynamic ductile fracture arrest in pipelines began in the late 1980s with a model that calculates the crack driving force in terms of CTOA as a function of crack speed.

The CTOA fracture criterion has now become one of the most promising fracture criteria used for characterising stable tearing in thin metallic materials. Initially, fracture resistance to crack extension was given by the Charpy energy, as in the Batelle Two-Curves method (BTCM) [41]. The Charpy test is related to crack initiation, bending of the specimen, and plastic deformation at the load points. It is necessary that tests performed to characterise the propagation resistance be able to isolate and quantify the propagation energy with respect to incremental crack advance. For this reason and due to the development of higher-strength steels with increased toughness and lower transition temperatures using controlled rolling techniques, the Charpy energy was replaced by drop-weight tear test (DWTT) energy in the HLP [42] and HLP Sumitomo [43] two-curves methods. DWTT tests are also related to crack initiation, bending of the specimen, and plastic deformation. However, notched DWTT specimens are larger than Charpy ones, and therefore relatively less of the total fracture energy is related to initiation. The statically pre-cracked DWTT showed the best compromise between isolating the propagation energy and ease of specimen preparation. Another step was the development of a test methodology to measure CTOA indirectly, derived on the basis of the difference in energy between two modified DWTT specimens with different initial crack lengths [44].

CTOA is defined from the crack growth resistance curve (R-curve) and particularly from the δ_R–Δa curve slope. This does not integrate fracture resistance to initiation, but only fracture resistance to crack extension. However, based on the CTOA, δ_R–Δa curve slope cannot be assumed as a material constant. For a better

agreement between the experimental and predicted curves, a bilinear form of CTOA should be used instead of the constant CTOA criterion (Fig. 22). Therefore the non-stable ductile crack extension can also be modelled. Non-stable crack extension affects few millimetres, while the stable one sometimes affects several metres.

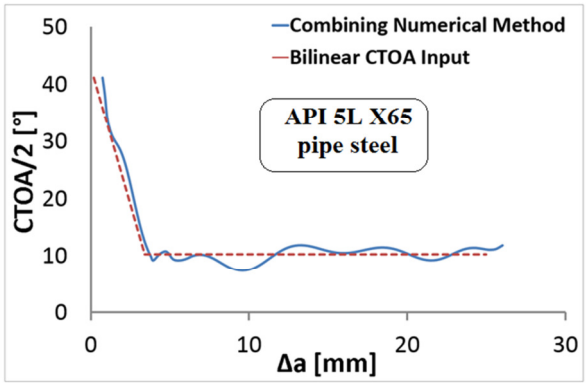

Fig. 22: Bilinear description of critical CTOA versus crack extension.

The critical CTOA is sensitive to geometrical parameters such as thickness or ligament size and loading mode through constraints, but this is a general problem for all fracture criteria.
The influence of geometrical parameters of pipes on CTOA has been proposed [7] and is given by the general form :

$$CTOA_c = C\left(\frac{\sigma_h}{E}\right)^m \left(\frac{\sigma_h}{\sigma_0}\right)^n \left(\frac{D}{t}\right)^q) \qquad (33)$$

where m, n, and q are dimensionless constants and C is expressed in degrees; σ_h is the hoop stress (MPa), σ_0 is the flow stress (MPa), D is the diameter (mm), and t is thickness (mm). The following values can be used for methane: C = 106, m = 0.753, n = 0.778 and q = 0.65. Therefore in a model based on $CTOA_{c;}$ leads to an influence of pipe diameter and thickness on crack velocity V_c and arrest pressure P_a.The crack velocity is expressed versus decompression wave pressure by Equation (34), where the parameters α, β and g depend on pipe diameter.

$$V_c = \alpha \,.\frac{\sigma_0}{\sqrt{R_f}} \,.\left(\frac{p_d}{p_a} - 1\right)^{\beta} \qquad (34)$$

Table 11 : 33 values of parameters α, β and γ of Equation (34), thickness 19 mm.

Pipe diameter	α	α	γ
355 mm	0.193	25.8	284.2
393 mm	0.14	24	290

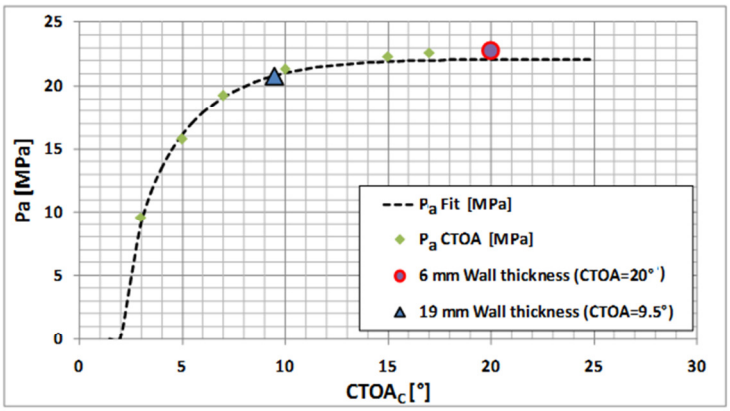

Fig. 23 : Influence of $CTOA_c$ on arrest pressure API 5L X 100 pipe steel

$CTOA_c$ has been determined on 6 mm thick test specimen and the thickness of the pipe is 19 mm. The influence of $CTOA_c$ on arrest pressure has been determined and results are presented in Fig. 23. The influence of thickness on arrest pressure for API 5L X65 pipe steel (pipe diameter) is small and about 12% in the range 6–19 mm: Table 12.

Table 12 : Influence of thickness on predictions of arrest pressure. Pipe with outer diameter D 393 mm made in API 5L X 65 pipe steel

Thickness (mm)	$CTOA_c$ (°)	Pa (MPa)
6	20	23.1
19	9.5	20.5

7. CONCLUSIONS

CTOA is a measure of fracture toughness. More precisely, it expresses the fracture resistance to ductile crack extension in radians or degrees. These units come naturally from the definition of the CTOA as the angle between the crack faces of a growing crack or as the slope of the R curve $\delta_R = f(a)$. However simple a definition, it exhibits some difficulty due to the irregular shape of the crack profile. The most appropriate methods follow the ASTM E2472-06e1 *Standard* [11] using an MDCB specimen and optical microscopy. An alternative method is to use the finite element method to fit experimental load-displacement diagrams mainly when the test temperature is low (it becomes difficult to carry out an optical examination of the specimen surface) or when the specimen is thick (due to the tunnelling effect).

Values of the CTOA are not intrinsic to materials. Like other measures of fracture toughness, it is sensitive to geometry and loading mode. This sensitivity can be described by a constraint parameter. For the thickness effect, the constraint parameter T_z is very appropriate.

CTOA is a good candidate to describe the fracture resistance of a ductile running crack. It represents only this resistance to crack extension and not a mixture of crack propagation and crack initiation energies. The use of this criterion requires a single parameter that can be obtained easily with a fracture test. Using the node release technique associated with the CTOA as a criterion for crack extension, numerical modelling is able to predict crack length and pressure at arrest.

REFERENCES

[1] Andersson H (1973). A finite element representation of stable crack growth. *J. Mech. Phys. Solids*, 21, 337–356.

[2] Rice JR, Sorensen EP (1978). Continuing crack tip deformation and fracture for plane-strain crack growth in elastic–plastic solids. *J. Mech. Phys. Solids*, 26, 163–186.

[3]. Shih CF, de Lorenzi HG, Andrews WR (1979). Studies on crack initiation and stable crack growth. *ASTM STP*, 668, 65–120.

[4] Kanninen MF, Rybicki EF, Stonesifer RB, Broek D, Rosenfield AR, Nalin GT (1979). Elastic–plastic fracture mechanics for two dimensional stable crack growth and instability problems. *ASTM STP*, 668, 121–150.

[5] Newman Jr JC (1984). An elastic–plastic finite element analysis of crack initiation, stable crack growth, and instability. *ASTM STP*, 833, 93–117.

[6] Brocks W, Yuan H (1991). Numerical studies on stable crack growth. In: *Defect Assessment in Components Fundamentals and Applications*, vol. 9. ESIS Publication, 19–33.

[7] Demofonti G, Mannucci G , Hillenbrand HG, Harris D. Evaluation of X100 steel pipes for high pressure gas transportation pipelines by full scale tests. *Int. Pipeline Conf.*, Calgary, Canada, 2004.

[8] Pluvinage G , Ben Amara M, Capelle J, Azari Z. Crack tip opening angle as a fracture resistance parameter to describe ductile crack extension and arrest in steel pipes under service pressure

[9] Cotterell B. "Slightly curved or kinked cracks", *International Journal of Fracture*, Vol.16, No. 2, April, 155-169, (1980).

[10] Erdogan F. and Sih, G.C."On the crack extension in plates under loading and transverse shear". *Transaction of the ASME. J.Basic Eng*, Vol 85 : 519-527, (1963).

[11] Capelle, J., Ben Amara, M., Pluvinage, G., Azari, Z. (2014) Role of constraint on the shift of ductile–brittle transition temperature of subsize Charpy specimens. Fatigue Fract. Eng. Mater. Struct. 37, DOI: 10.1111/ffe.12212.

[12] Darcis PhP, McCowan CN, Windhoff H, McColskey JD, Siewert TA, "Crack tip opening angle optical measurement methods in five pipeline steels", Engineering Fracture Mechanics, 75: 2453-2468, 2008.

[13] G. Pluvinage, J. Capelle, and M. Hadj Méliani. " A review of fracture toughness transferability with constraint" Applied Mechanics, Behavior of Materials, and Engineering systems - Selected papers from 5th Algerian Congress of Mechanics, CAM2015, October 25 – 29, El-Oued, Algeria Editor(s) name(s): Boukharouba T., Pluvinage G., Azouaoui K, (2015).

[14] W. Lloyd et F.McClintock, « Microtopography for ductile fracture process characterization Part 2: application for CTOA analysis », Engineering Fracture Mechanics, vol. 70, no. 3-4, p. 403-415, févr. 2003.

[15] D. Dawicke et M. Sutton, « CTOA and crack-tunneling measurements in thin sheet 2024-T3 aluminum alloy », Experimental Mechanics, vol. 34, no. 4, p. 357-368, déc. 1994.

[16] J. Heerens et M. Schödel, « On the determination of crack tip opening angle, CTOA, using light microscopy and δ5 measurement technique », Engineering fracture mechanics, vol. 70, no. 3-4, p. 417-426, 2003.

[17] M. Ben amara [1], J.Capelle [1], Z.Azari [1], G.Pluvinage [2]
The application of CTOA criterion to simulate crack propagation and arrest in a modified CT test specimen NT2F14

[18] S. Xu, N. Petri, et W. R. Tyson, « Evaluation of CTOA from load vs. load-line displacement for C(T) specimen », Engineering Fracture Mechanics, vol. 76, no. 13, p. 2126-2134, sept. 2009.

[19] S. Xu, R. Bouchard, et W. R. Tyson, « Simplified single-specimen method for evaluating CTOA », Engineering fracture mechanics, vol. 74, no. 15, p. 2459-2464, 2007.

[20]. Newman JC, James MA, Zerbst U (2003). A review of the CTOA/CTOD fracture criterion. *Engng Fract. Mech*., 70, 371–385;

[21]. Xu S, Bouchard R, Tyson WR (2007). Simplified single-specimen method for evaluating CTOA *Engng Fract. Mech*., 74, 2459–2464

[22]. Martinelli A, Venzi S (1996). Tearing modulus, J-integral, CTOA and crack profile shape obtained from the load–displacement curve only. *Engng Fract. Mech*., 53, 263–277.

[23]. Jian Fang, Jianwei Zhang, Lei Wang (2014). Evaluation of cracking behavior and critical CTOA values of pipeline steel from DWTT specimens. *Engng Fract. Mech*., 124/125, 18–29.

[24]. ASTM E2472-06e1 (2002). Standard Test Method for Determination of Resistance to Stable Crack Extension under Low-Constraint Conditions.

[25]. O'Donoghue PE, Kanninen MF, Leung CP, Demofonti G, Venzi S (1997). The development and validation of a dynamic fracture propagation model for gas transmission pipelines. *Int. J. Press. Vessels Pip.*, 70, 11–25

[26]. Darcis Ph.P, McCowan CN, Windhoff H, McColskey JD, Siewert TA (2008). Crack tip opening angle optical measurement methods in five pipeline steels. *Engng Fract. Mech*., 75, 2453–2468.

[27]. Amaro RL, Sowards JW, Drexler ES, McColskey JD, MacCowan C (2013). CTOA testing of pipe line steels using MDCB specimens. *J. Pipe Engng*, 3,199–216.

[28]A. S. Gullerud, R. H. Dodds, R. W. Hampton, et D. S. Dawicke, « Three-dimensional modeling of ductile crack growth in thin sheet metals: computational aspects and validation », Engineering Fracture Mechanics, vol. 63, no. 4, p. 347-374, 1999.
[29]R. W. Hampton et D. Nelson, « Stable crack growth and instability prediction in thin plates and cylinders », Engineering Fracture Mechanics, vol. 70, no. 3-4, p. 469-491, févr. 2003.
[30]Zerbst, Uwe a Heinimann, MarkusbDalle Donne, ClaudiocSteglich, Dir, « Fracture and damage mechanics modelling of thin-walled structures – an overview", Engineering Fracture Mechanics (2007) Elsevier
[31] W Maxey, "Dynamic crack propagation in line pipe", In: Analytical and Experimental, Fracture Mechanics, ed. Sih G.C and Mirabile M: 109-123, (1981).
[32] A. Pirondi et D. Fersini, « Simulation of ductile crack growth in thin panels using the crack tip opening angle », Engineering Fracture Mechanics, vol. 76, no. 1, p. 88-100, janv. (2009).
[33] F.Oikonomidis, A.Shterenlikht, and C.E. Truman. "Prediction of crack propagation and arrest in x100 natural gas transmission pipelines with the strain rate dependent damage model (SRDD). part 1 : A novel specimen for the measurement of high strain rate fracture properties and validation of the SRDD model parameters. International Journal of Pressure Vessels and Piping, 105 :60–68, (2013).
[34] Espen Jakobsen, "Deformation of pressurized pipelines", Master Thesis, Norwegian University of Science and Technology, (2013).
[35] M. Civallero, M. Mirabile, and G.C Sih." Fracture mechanics in pipeline technology. Analytical and Experimental FractureMechanics", Ed. Sih, G.C and Mirabile.M,: 157–174, (1981).
[36] Cheng Cen. "Characterization and Calculation of Fracture Toughness for High Grade Pipes". PhD thesis, University of Alberta, (2013).
[37] R. Eiber, T. Bubenik, and W. Maxey, " GASDECOM, computer code for the calculation of gas decompression speed that is included in fracture control technology for natural gas pipelines. NG-18 Report 208," American Gas Association Catalog,(1993).
[38] MA James and JC Newman. The effect of crack tunnelling on crack growth : experiments and CTOA analyses. Engineering Fracture Mechanics, 70 (3) :457–468, (2003).
[39] I.Scheider, M Schödel, W Brocks, and W Schönfeld. "Crack propagation analyses with ctoa and cohesive model" : Comparison and experimental validation. Engineering Fracture Mechanics, 73(2) :252–263, (2006).
[40] Dinh Cuong Tran. Interaction rupture-flambage, le cas du «splitting» de tube métallique : Approche expérimentale et numérique. PhD thesis, INSA de Lyon, (2013).
[41] W. A Maxey. 5th Symp. on Line Pipe Research, PRCI Catalog No. L30174, Paper J, 16.
[42] E. Sugie, M. Matsuoka, H. Akiyama, T. Mimura, Y. Kawaguchi, "A study of shear crack-propagation in gas-pressurized pipelines", J. Press. Vess. – T. ASME 104, (4) : 338–343, (1982).
[43]R.Higuchi, H. Makino, I .Takeuchi. "New concept and test method on running ductile fracturearrest for high pressure gas pipeline". In: 24th World Gas Conf., WGC 2009, Vol. 4, International Gas Union, Buenos Aires, Argentina : 2730–2737,(2009).
[43] Demofonti G, Buzzichelli G, Venzi S, Kanninen M (1995). Step by step procedure for the two specimen CTOA test. In: Denys R (ed.). *Pipeline Technology*, vol II. Elsevier.G.